

Photon-Memristive System for Logic Calculation and Nonvolatile Photonic Storage

Ke Zhang, Dehuan Meng, Feiming Bai,* Junyi Zhai,* and Zhong Lin Wang*

Memristor-based architectures have shown great potential for developing future computing systems beyond the era of von Neumann and Moore's law. However, the monotonous electrical input for dynamic resistance regulation limits the developments of memristors. Here, a concept of a photon-memristive system, which realizes memristance depending on number of photons (optical inputs), is proposed. A detailed theoretical derivation is performed and the memristive characteristics, as stimulated by the optical inputs based on a hybrid system, consisting of a low-dimension photoelectric semiconductor and a ferroelectric substrate are determined. The photon-memristive system is also suitable for nonvolatile photonic memory since it possesses three or more-bit data storage, desirable resistance-change space, and an ON/OFF ratio of nearly 10^7 . The integrated circuit based on several photon-memristive systems also realizes available photon-triggered in-memory computing. The photon-memristive system expands the definition of memristors and emerges as a new data storage cell for future photonic neuromorphic computational architectures.

are the prerequisites of realizing photonic computing systems. In the electronic circuits, the memristor, behaving like a non-linear and dynamic resistor with memory depending on the past historical electrons signals, has been developed since it was postulated by Chua in 1971.^[3–11] However, little effort applied to developing a memristive system stimulated by using optical inputs (photon is the main governing factor), such as a photon-memristive system (PMS). Combining the resistors and optical inputs, a PMS should be a continuously tunable resistor with the memory ability to record the historical number of photons (n) in simple terms. In other words, the memristance (M) is dynamically determined by the number of photons (n) and retained when the optical inputs are removed. By introducing optical regulations to memristors instead of traditional electrical regulations, a PMS could

1. Introduction

Photons are excellent carriers of quantum information for future super-speed computing and ultra-large capacity storage.^[1,2] Programming and recording for photons signals

have significant importance in future photonic storage, optical computing, and artificial neural networks. For example, the integrated circuits based on PMSs have the potential to be used for photon-triggered logic gates that combine binary computing and data storage. Considering a PMS as the basis of hardware is expected to realize high speed, high parallel, low consumption, and large capacity computation and storage.

The question, therefore, is how one can achieve a PMS. A composite architecture consisting of resistance-changing materials and photoelectric materials is a good approach. Ferroelectric materials, such as $\text{Pb}(\text{Zr}_{1-x}\text{Ti}_x)\text{O}_3$ (PZT) and BiFeO_3 (BFO),^[12–14] have variable resistances depending on the polarization switching by applying a voltage pulse with an amplitude above the coercive bias. On this basis, a ferroelectric field-effect transistor (FeFET) is a nonvolatile memory transistor that uses a ferroelectric material as the gate insulator, and it possesses excellent features as an integrated memory cell, such as nonvolatility, better scalability, higher read-write speeds, lower dissipation powers, higher tamper resistances, and higher radioactivity tolerance.^[15–17] Therefore, ferroelectric materials and FeFETs could be the basic building block of PMSs. In addition, a medium for optical stimulations is necessary. Transition-metal dichalcogenides (TMDs) are a kind of layered photoelectric semiconductor material with a high surface-to-volume ratio and outstanding electronic and optoelectronic properties,^[18–20] especially at the atomic thickness scale. Rich and tunable electronic band structures,^[21] controllable interface states,^[22] and superior photoelectric conversion

Dr. K. Zhang, Prof. J. Zhai, Prof. Z. L. Wang
CAS Center for Excellence in Nanoscience
Beijing Key Laboratory of Micro-Nano Energy and Sensor
Beijing Institute of Nanoenergy and Nanosystems
Chinese Academy of Science
Beijing 100083, P. R. China
E-mail: jyzhai@binn.cas.cn

Dr. K. Zhang, Prof. J. Zhai, Prof. Z. L. Wang
College of Nanoscience and Technology
University of Chinese Academy of Sciences
Beijing 100049, P. R. China

Dr. D. Meng, Prof. F. Bai
State Key Laboratory of Electronic Thin films and Integrated Devices
University of Electronic Science and Technology of China
Chengdu 610054, P. R. China
E-mail: fmbai@uestc.edu.cn

Prof. Z. L. Wang
School of Material Science and Engineering
Georgia Institute of Technology
Atlanta, GA 30332, USA
E-mail: zlwang@gatech.edu

The ORCID identification number(s) for the author(s) of this article can be found under <https://doi.org/10.1002/adfm.202002945>.

DOI: 10.1002/adfm.202002945

capabilities^[23] make it possible for monolayer TMDs to be a favorable medium for realizing PMSs that are stimulated by optical inputs. Above all, a feasible idea is to introduce optical stimulations by using a photoelectric material to change the polarization of the ferroelectric material, which gate-controls the channel resistance in turn. The ferroelectric/photoelectric hybrid system is expected to realize the PMS with variable resistance depending on the photons.

In this paper, we first propose a concept of the PMS and show the theoretical relationships between the memristance (M) and the number of photons (n). Simultaneously, a PMS is fabricated based on a MoS₂/PZT heterostructure, and it possesses the potential for nonvolatile photonic storage and logic calculation. In our design, the electric field at the interface of the MoS₂ and PZT induced by photon excitation changes the intensity and direction of the ferroelectric polarization the of PZT film. The PMS can be incorporated between the high resistance state (HRS) and low resistance state (LRS) with continuous internal resistance states to record the pre-applied photons. Using energy band structure and ferroelectric domain dynamic models, we explain photon-induced ferroelectric domains propagation and derive a mechanism for the photon-memristive effect in a PMS. In terms of the applications, various optical erasing and writing are accomplished based on the MoS₂-PZT structure by exerting an ephemeral illumination on the MoS₂ channel with different times and intensities. PMS not only has simplest construction but also high and balanced performances compared to previous optical memory devices,^[24] such as high ON/OFF ratio (nearly 10⁷), multiple bits (3-bit or more) nonvolatile photonic storage, and retention time (>10⁴ s). The logic integrated circuits based on PMSs are suitable for photon-triggered in-memory computing. Our results suggest that PMSs may emerge as a new class of memristive system with tremendous potential to serve as the basis of the hardware in future photonic information technology.

2. Concept and Model of the PMS

In 1971, Chua theoretically stated that there should be four basic circuit elements, resistors, inductors, capacitors, and memristors, and described the relations between the electric fundamental circuit variables of the current (i), voltage (v), charge (q), and magnetic flux (φ). Among them, the memristor, with memristance of M , provides a functional relation between q and φ as $d\varphi = Mdq$. Until now, there has not been a memristor connecting q and φ . In most cases, a memristor is a two-terminal electrical component that can use numbers of charges that flow through the device to tune the resistance. That is, M is a function of q . However, four fundamental variables restrict the diversification of the developments of memristors and memristive systems. In this paper, we introduce a new variable, the number of photons n , as a substitute for q , and propose a new concept of the PMS, as shown in Figure 1a. The PMS builds the relationships between M and n and it can be realized by using an integrated system consisting of a resistor, a capacitor, and light/photons. The physical model of the PMS uses a light tuning capacitor to determine the resistor status, thus realizing memristive characteristics. Figure 1b shows the mechanism of memorized states switching based on this model. We use an N-type channel as the resistor and ferroelectric film as the capacitor. In this PMS, ferroelectrics with downward (upward) polarization deplete (enhance) the electrons in the N-type channel, resulting in HRS (LRS). The photons are expected to induce an electric field at the interface between the resistor and capacitor, which could change the ferroelectric polarization, thereby achieving random and reversible switching between HRS and LRS. Most importantly, the resistance could be maintained after the light is turned off. Therefore, M could be a function of n .

According to the modulation mechanism, if LRS → HRS, then

$$I_{ds} = \frac{W}{L} \mu [P^* - C_i (V_p - V_T)] V_{ds} \quad (1)$$

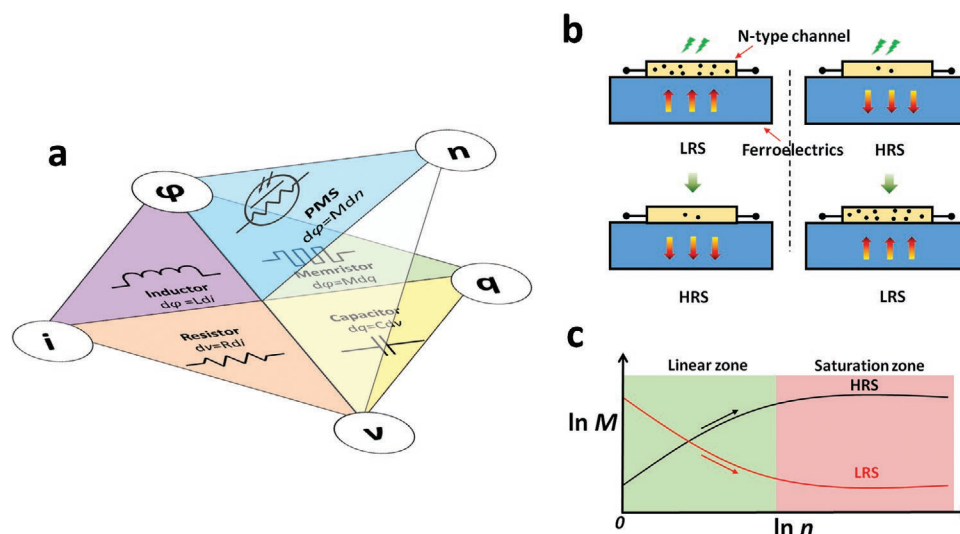


Figure 1. Concept and model of the PMS. a) The four fundamental circuit elements, including the inductor, resistor, capacitor, and memristor, are described by using the relations between the variables of the electric current (i), voltage (v), charge (q), and magnetic flux (φ). By introducing the number of photons (n) as a substitute for q , a new circuit element, the PMS, is proposed that describes the relation between the variables φ and n . b) The PMS structural models in the HRS and LRS. c) Simulated relationships between M and n in the PMS according to theoretical deduction.

$$V_p = \frac{\sigma \cdot d}{2\epsilon_0} = \frac{\alpha n \cdot d}{2\epsilon_0 W L} \quad (2)$$

$$M_{\text{LRS} \rightarrow \text{HRS}} = \frac{V_{\text{ds}}}{I_{\text{ds}}} = \frac{1}{\frac{W}{L} \mu (P^* + C_i V_T) - \frac{\mu \alpha C_i d}{2\epsilon_0 L^2} n} = \frac{1}{B - An} \quad (3)$$

where

$$A = \frac{\mu \alpha C_i d}{2\epsilon_0 L^2}, B = \frac{W}{L} \mu (P^* + C_i V_T) \quad (4)$$

and W and L are the channel width and length, respectively. V_p and V_T are the photon-induced voltage and coercive voltage of the ferroelectrics, respectively. C_i is the gate capacitance, σ is the trapped charge density, μ is the electron mobility, d is the ferroelectric thickness, ϵ_0 is the vacuum permittivity, and α is the conversion ratio between the number of photons and the trapped charge. In addition, we define the maximum upward polarization as P^* and the maximum downward polarization as 0.

If HRS \rightarrow LRS, then

$$I_{\text{ds}} = \frac{W}{L} \mu [C_i (V_p - V_T)] V_{\text{ds}} \quad (5)$$

$$M_{\text{HRS} \rightarrow \text{LRS}} = \frac{V_{\text{ds}}}{I_{\text{ds}}} = \frac{1}{-\frac{W}{L} \mu C_i V_T + \frac{\mu \alpha C_i d}{2\epsilon_0 L^2} n} = \frac{1}{An - C} \quad (6)$$

where

$$A = \frac{\mu C_i d}{2\epsilon_0 L^2} \text{ and } C = \frac{W}{L} \mu C_i V_T \quad (7)$$

Therefore, there is an inverse function between M and n in our PMS. In logarithmic coordinates

$$\ln M_{\text{LRS} \rightarrow \text{HRS}} = -\ln(B - An) \quad (8)$$

$$\ln M_{\text{HRS} \rightarrow \text{LRS}} = -\ln(An - C) \quad (9)$$

We conclude that $\ln(M)$ is linearly correlated with $\ln(n)$. When the ferroelectric polarization reaches saturation, M is constant. The simulated curves are presented in Figure 1c.

3. Fabrication and Characterization of the PMS

We began the fabrication of the PMS (Figure 2a,b) by using chemical vapor deposition (CVD)^[25] to grow large-scale, single-layer MoS₂ as the photoelectric material and resistor. A 10 nm thick Pb(Zr_{0.52}Ti_{0.48})O₃ (PZT) epitaxial film was grown on the (001)-oriented SrTiO₃ (STO) single-crystal substrates by using pulsed-laser deposition (PLD). Then, monolayer MoS₂ flakes were transferred to the PZT/STO substrate and electrical contacts were fabricated using electron-beam lithography followed

by the deposition of 50 nm thick gold electrodes (with 5 nm thick chromium as the adhesion layer). During the PMS measurements, a high precision manual translation table and a microscope combined with a charge-coupled device imaging system were used to precisely localize the device (Figure S1, Supporting Information). For laser wavelength, the excitation source is required to be able to excite the photogenerated carriers in monolayer MoS₂ ($\lambda \leq 688$ nm) but not affect the polarization of PZT thin film ($\lambda \geq 342$ nm). In this paper, a focused laser beam ($\lambda = 532$ nm) served as the excitation source for the photon-memristive behaviors. The width of the MoS₂ channel is 10 μm , and the light spot has a diameter of 3 μm . The broad working space and accurate and visible micro-operations ensure that the laser only illuminates the MoS₂ channel. Before operating the PMS device, a series of material characterizations of the MoS₂ and PZT/STO substrate were carried out. The typical Raman positions of the MoS₂ on the PZT/STO substrate between the A1 g and E1 2 g peaks have a ≈ 21 cm⁻¹ frequency difference, thereby reflecting its monolayer characteristic.^[26,27] The PZT/STO substrate has no obvious Raman peaks within the wave range of 370–420 cm⁻¹ (Figure S2, Supporting Information). The deposited PZT thin film has an ultraflat surface with the roughness of ≈ 0.25 nm (Figure S3, Supporting Information), which is beneficial to the micro-nanomachining and electrical performance of atomic thin 2D material-based optoelectronics. PZT is a good dielectric with a large bandgap of 3.63 eV,^[28] meaning that only the MoS₂ has a photoresponse that is excited by the 532 nm laser (photon energy: 2.33 eV). We assess the photoresponse of the MoS₂ on the PZT/STO substrate in the as-fabricated state under dark and illuminated conditions (Figure S4, Supporting Information). Obvious photocurrent enhancement is observed when the MoS₂ channel is illuminated with increasing laser power, thereby indicating a favorable photoresponse. The MoS₂-PZT PMS operates by applying a 532 nm focused laser and a constant drain-source voltage (V_{ds}) in the configuration that is shown in Figure 2b. Next, the photon-memristive behaviors based on the MoS₂-PZT PMS are achieved by coordinating the illumination and applied source-drain voltage (Figure 2c). As an as-fabricated PMS, a simple reset operation is required. A 10 V bias is applied to start (stage a) and is followed by exerting illumination (532 nm laser, $P = 1.05$ mW) for 10 s (stages b,c). This process cleans the residual stored states. After being reset, the PMS is electrically read at a 1 V bias in the dark and the device exhibits an ultralow drain current (I_{ds}) of ≈ 0.1 nA (stage d) corresponding to an HRS (OFF state). Subsequently, the memory cell is optically set by illuminating the MoS₂ channel (532 nm laser, $P = 1.05$ mW) for 10 s (stage e). As observed, the drain current rapidly increases by more than 4 orders of magnitude and reaches saturation (≈ 5 μA) corresponding to an LRS (ON state). After removing the illumination, the current does not sharply return to its origin state, but slowly decreases (stage f) and maintains a stable LRS for a long time. Figure 2d shows the retention time of the readout currents after the optical reset and set processes, respectively. The PMS exhibits highly reliable readout current ($V_{\text{read}} = 1$ V) retention characteristics over several hours in both the LRS and the HRS. An appreciable LRS/HRS (ON/OFF) ratio of $\approx 10^3$ could still be maintained after 10^4 s. Distinguishing and steady resistance states suggest that

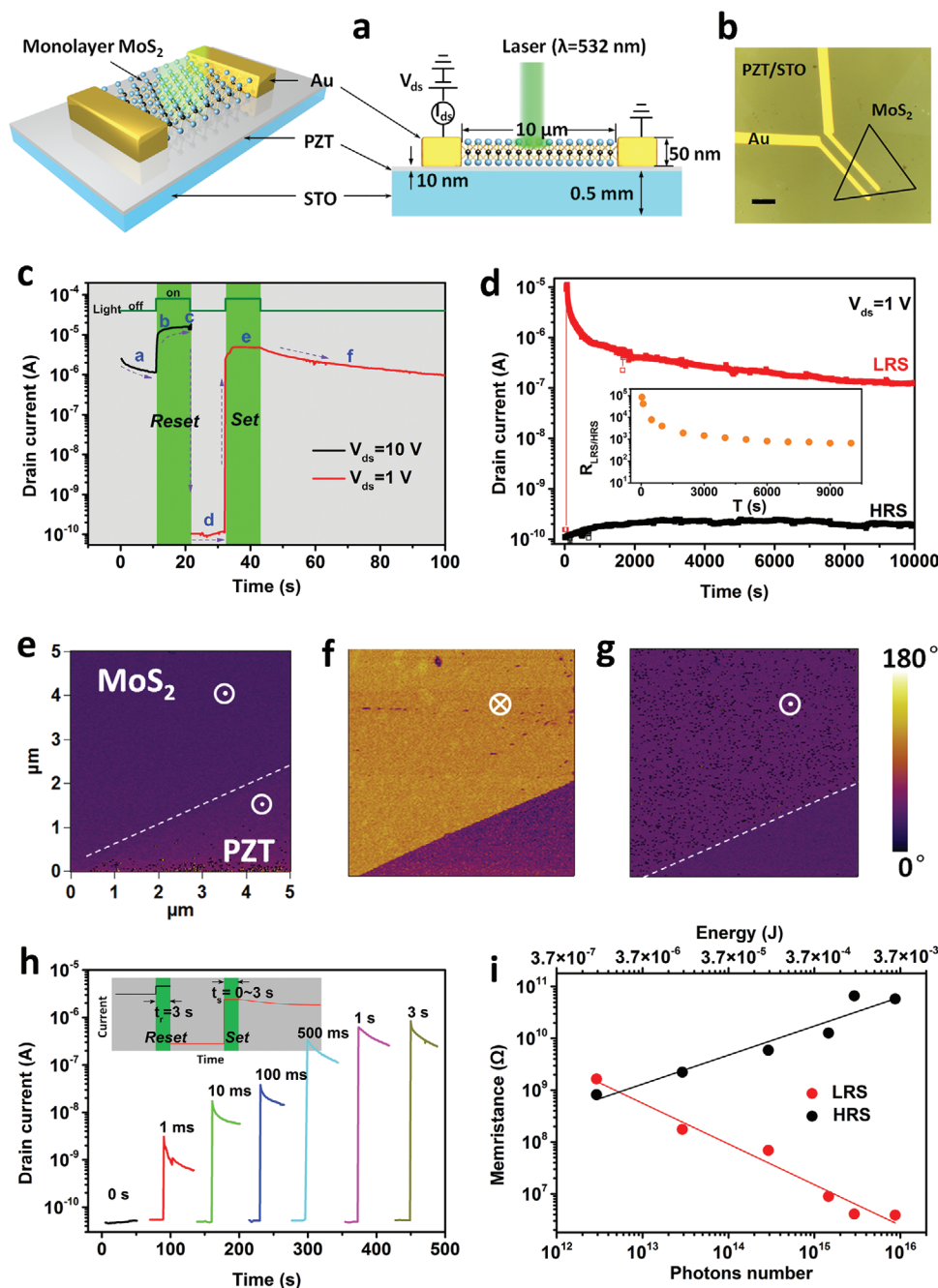


Figure 2. Demonstration of the PMS based on a MoS₂-PZT hybrid system. a) Schematic of the MoS₂-PZT PMS architecture and the focused laser beam that are used to probe the device and cross-sectional view of the structure of the MoS₂-PZT memory cell with the electrical connections and illumination that are used to characterize the device. b) The optical image of PZT-MoS₂ PMS. The scale bar is 20 μm. c) Readout current variations of the PZT-MoS₂ PMS before, during and after the reset and set processes. d) Retention characteristics of the MoS₂-PZT PMS. Both the OFF- and ON-state currents are read at V_{ds} = 1 V. The inset is the ON/OFF ratio at different time points. e–g) The PFM images in the MoS₂-PZT junction over a fixed area (5 × 5 μm) between the drain and source electrodes at different stages. e) In the original stage. f) After the reset operation. g) After the optical set process. h) Readout current as a function of the optical set time (t_s) from 0 to 3 s. The inset is a parametric model. i) The memristance dependence on the number of photons and the photon energy according to the experimental data in logarithmic coordinates.

MoS₂-PZT PMS is promising to realize the memristive effect that is stimulated by optical inputs. The memorized resistance and abrupt transition between the LRS and HRS are certainly related to the polarization of the PZT. We examine the out-of-plane polarization states of the PZT using single-frequency

piezo force microscopy (PFM). Here, a fixed area between the drain and source electrodes was selected to acquire the PFM images. In its original state, there is nearly no phase difference between the monolayer MoS₂ region (on PZT film) and the bare PZT region (Figure 2e). Due to the absence of a bottom

electrode, the PZT shows a preferred upward out-of-plane polarization (P_{\uparrow})^[29,30] that is toward the MoS₂. Next, a reset operation is executed ($V_{ds} = 10$ V, $P = 1.05$ mW, and $t_r = 10$ s) and followed by obtaining the PFM scanning image over the same area (after waiting for 5 min after the reset process). It can be seen that the PZT film that is covered by the MoS₂ exhibits a conspicuous phase transition, while the bare PZT film has no change (Figure 2f). In this case, the net polarization of the PZT film underneath the MoS₂ switched from upward to downward, which leads to a low readout current (HRS) between the drain and source. Finally, a specified optical set operation is applied to the device ($P = 1.05$ mW and $t_s = 10$ s), which is followed by acquiring the PFM images over the same area (after waiting for 5 min after the set process). As shown in Figure 2g, the PFM phase of the PZT underneath the MoS₂ at this point has an abrupt transition demonstrating a significant reduction of the net downward polarization due to the rotation of the ferroelectric domains. That is, optical excitation induces an opposite polarization reversal of the PZT, thus significantly increasing the drain current (LRS). We conclude that the transition and retention of the memristance in the PMS are attributed to the change of the PZT polarization that is controlled by optical inputs, which are photons. We try to prove the functional relationships between M and n . As shown in Figure 2h; and Figure S5 (Supporting Information), we examine the memristive behaviors using the variable n for the illuminated MoS₂ channel by changing the illumination time (set time, t_r and reset time, t_s) in the reset and set processes. Figure 2h shows the readout current that is measured after illumination as a function of t_s from 0 to 3 s. Due to the same reset operation ($V_{ds} = 10$ V, $P = 1.05$ mW, and $t_r = 3$ s), the OFF-state current is constant. As observed, the readout ON-state current decreases as t_s increases in the set process. Similarly, the OFF-state current dependence on t_r is also displayed in Figure S5 (Supporting Information). In particular, a fast optical set and reset with a time of 1 ms still achieves an On/Off ratio of $\approx 10^2$, which is acceptable for many practical applications. The changes of the resistances that are stimulated by the photon inputs are estimated according to the light pulse time dependence in Figure 2h; and Figure S5 (Supporting Information). We evaluated n by using the formula $n = \frac{P \cdot t}{h\nu}$, where P is the light power, t is the time of the light pulse, h is the Planck constant, and ν is the photon frequency. Figure 2i shows the relevant results of M and n (or the corresponding photon-excited energy) in the experiments. M is linearly correlated with n in both processes (LRS→HRS and HRS→LRS), which agrees with the theoretical deductions.

4. Analysis of the Physical Mechanism

These observations and analyses can be explained by the following underlying physical mechanism of the photon-memristive effect. To plainly illustrate it, each stage is analyzed by using an energy band diagram at the MoS₂-PZT interface and a simple model of the polarization state in the PZT (Figure 3a–d). The CVD-grown monolayer MoS₂ has an N-type characteristic and a 1.8 eV direct bandgap.^[31,32] The PZT has a larger bandgap

of 3.63 eV without absorption using a 532 nm laser. A large-scale MoS₂ flake is appressed to the PZT thin layer by van der Waals forces, thereby forming a type I heterostructure at the interface according to the embedding energy level distributions (Figure 3a). The spontaneous upward polarization (P_{\uparrow}) of the PZT drives the conduction band of the MoS₂ at interface approaching the Fermi level. In the thermal equilibrium state, a barrier spike (≈ 0.7 eV) exists in the junction of the valence bands (Figure 3b). When the MoS₂ channel is illuminated, the photo-generated electrons and holes are separated by a built-in electric field (E_{in} , MoS₂→PZT) at the interface of the MoS₂ and PZT on account of the work-function mismatch of the Fermi levels. The photogenerated electrons could recirculate in the external circuit, but the holes with energy of ≈ 0.53 eV ($\epsilon_{hole} = \epsilon_{laser} - \epsilon_{gap}$) are unable to skip barrier (≈ 0.7 eV) and are instead pushed into the potential well. These intensive positive charges accumulate near the interface and create a strong out-of-plane electric field (E_p), which has been proven in our previous work,^[33] leading to the polarization switching in the PZT underneath the MoS₂. Most ferroelectric domains turn downward and produce a net out-of-plane downpolarization (P_{\downarrow}). After removing the illumination and bias voltage simultaneously, such downpolarization is preserved (Figure 3c). Considering the N-type channel, negatively charged electrons are the major transport carriers. Negative polarization charges on the top surface of the PZT expel the electrons in the MoS₂ channel. This results in the downshift of the Fermi level (Figure 3c) and a great increase in the channel resistance, thereby causing an ultralow stable OFF-state current (HRS). However, the shift of the MoS₂ Fermi level results in the reconstruction of the band structure at the interface. A new potential well (≈ 1.13 eV) appears in the conduction band joint and an inversive built-in electric field (E_{in}' , PZT→MoS₂) forms at the interface (Figure 3d). Due to an extremely low electron concentration, many photon-excited electrons in the optical set process converge into the new potential well, thereby forming an opposite and larger vertical out-of-plane electric field (E_n). Such an electric field results in the reversal of a number of ferroelectric domains, significantly reduces the former net downpolarization and transforms into the net uppolarization (P_{\uparrow}). Consequently, the Fermi level of the MoS₂ moves toward the conduction band and increases the channel's electron concentration (Figure 3a). As the set operation ends (removing the illumination), the reversed polarization is retained and leads to a persistent high readout ON-state current (LRS) until the next reset operation. By the way, the observed slow descent of the photocurrent at the beginning (stage f, Figure 2c) may be due to the compensation of the interfacial charges due to substrate-bound water, as mentioned in previous studies,^[34,35] but it is not the dominant factor in the large resistance difference between the HRS and LRS, as shown in Figure S6 (Supporting Information).

5. Multibit Nonvolatile Photonic Storage and Logic Operation

Based on the above physical mechanism, the MoS₂-PZT PMS will have attractive application values in the fields of multibit photonic data storage because of the ultralow dark current,

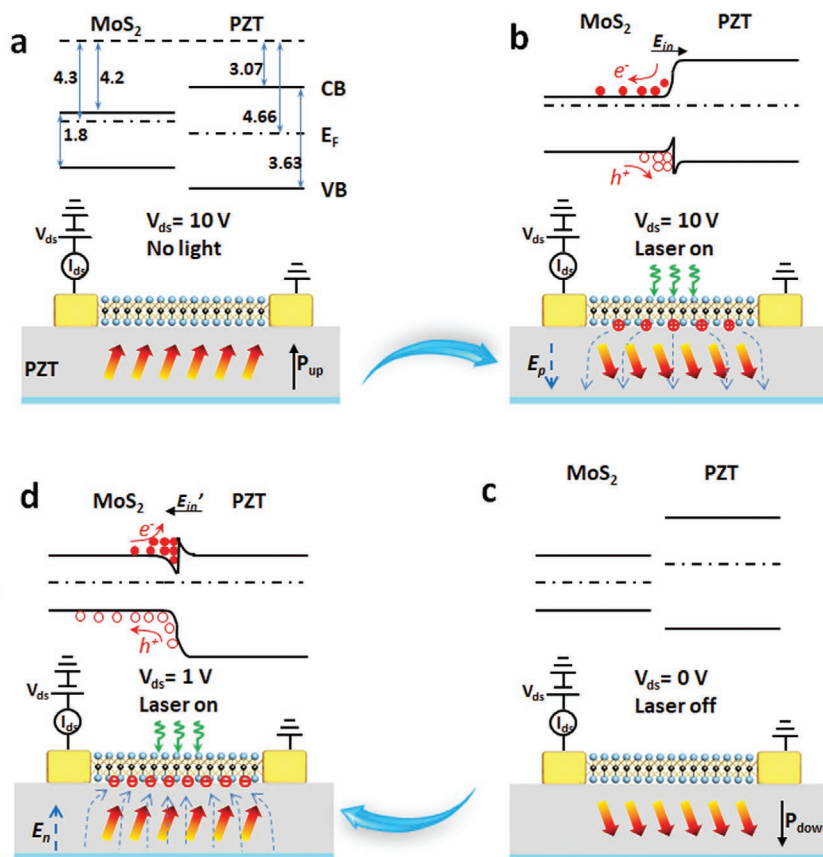


Figure 3. Mechanism of the photon-memristive effect in PMS. a–d) Energy band diagrams at the MoS₂-PZT interface and the matched polarization state models of the PZT underneath the MoS₂ at different processes, including the initial state a), optical reset process b), after optical reset c), and optical set process d).

high ON/OFF ratio and long retention time. After a fixed erasing operation (reset process) ($V_{ds} = 10$ V, $P = 1.05$ mW), an OFF-state readout current of ≈ 0.1 nA is achieved at $V_{ds} = 1$ V, which is defined as “0” (Figure 4a, black line). By varying the illumination power in the writing operation (set process), different optical signals are written to the MoS₂ channel, which are defined as “1,” “2,” and so on (Figure 4a, colored lines). With the increasing laser power, the ON-state readout current also gradually increases. It is easy to understand that the light with higher power excites more photogenerated carriers and more electrons are trapped at the interface, which generates a stronger vertical field that induces more ferroelectric domains’ reversal in the PZT underneath the MoS₂. Hence, different polarization conditions change the resistance of the MoS₂ channel, leading to various data storage levels. In our experiment, eight readout current levels (“0”–“7”) are used to achieve 3-bit data storage. It should be noted that higher bit (>3-bit) data storage can be realized by expanding and subdividing the laser power distributions. We next discuss the potential of the PMS in continuous data writing and data erasing (Figure 4b). By using optical write/erase operations with varying laser power, we are able to orderly and reliably move between these intermediate memorized states with high repeatability. From the HRS to LRS, simple optical writing with increasing laser power allows continuous intermediate states to transition.

From the LRS to HRS, these intermediate states could be quascontinuously reached by varying the laser power and by using a constant high bias (partial erasing) instead of a second data writing after fully erasing the data. In addition to illumination, the erasing and reading voltages are also the key parameters in practical applications, which play an important synergic role in determining the photonic storage characteristics. An MoS₂-PZT PMS with an ≈ 15 μm channel is used to demonstrate the erasing/reading voltage dependence so that the OFF-state current could be further reduced to achieve a higher ON/OFF ratio. Under the premise of utilizing a constant writing operation and reading voltage (1 V), we vary the erasing voltage (laser power is constant) from 15 to 1 V and the read OFF- and ON-state currents (Figure S7, Supporting Information). Obviously, the erasing voltage has a big influence on the OFF-state current level but little change on the ON-state current. In detail, with the decreasing erasing voltage, the PMS performs an increasing OFF-state current, thus resulting in the degressive ON/OFF ratio (Figure 4c, left). For $V_{ds} = 15$ V in the erasing operation, the OFF-state current is too small (below 10^{-3} pA) for precise detection, thereby leading to an ultrahigh ON/OFF ratio approaching $\approx 10^7$. In contrast, there is little memory effect when the erasing voltage is set to 1 V. This result may be ascribed to the assistance of the high in-plane voltage for photon-excited carriers. At a high bias, asymmetric schottky

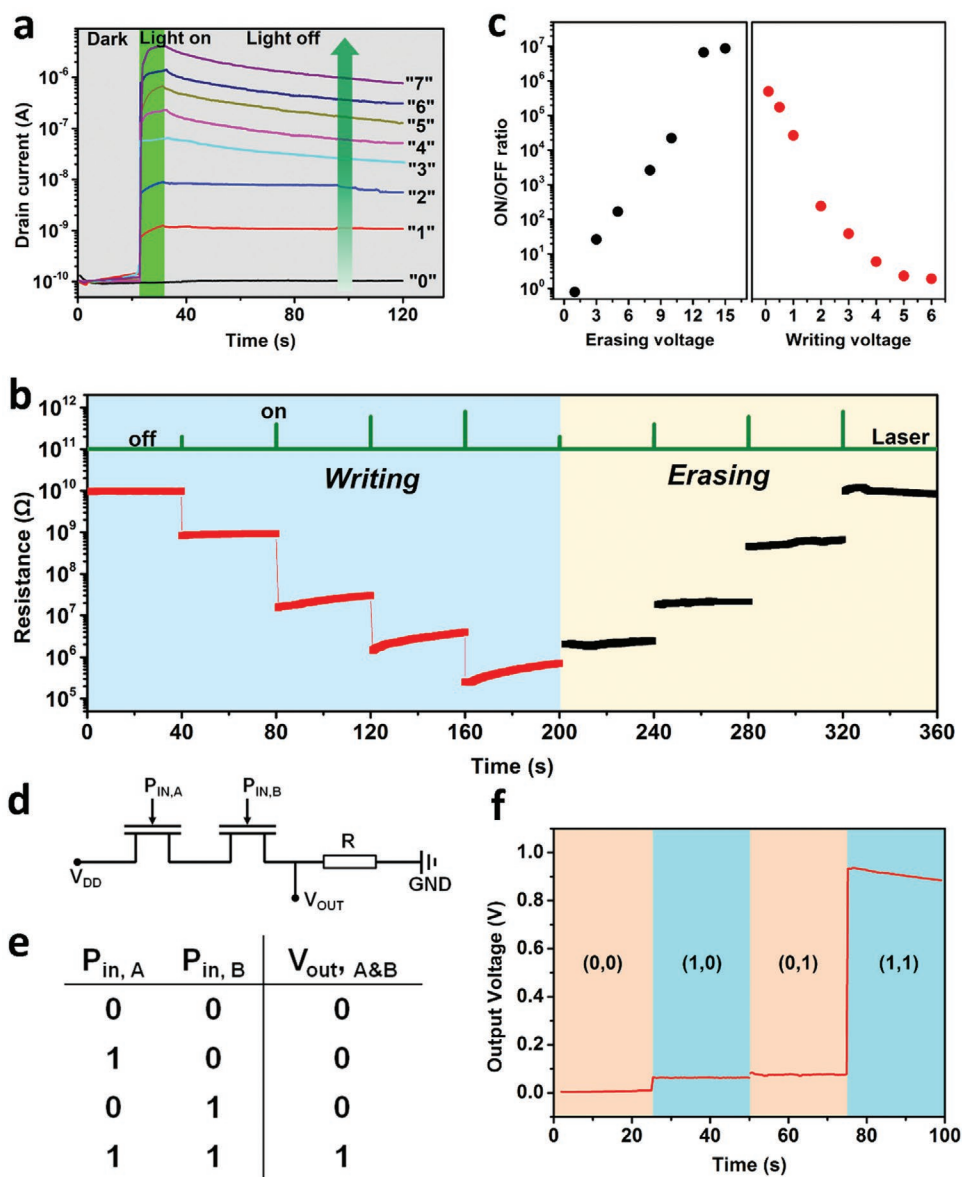


Figure 4. Multibit nonvolatile photonic storage and logic operation. a) Eight optical programmed states ("0"–"7") for three-bit data storage. The "0" readout state ($V_{ds} = 1$ V) is the OFF-state (absence of optical writing). The "1"–"7" readout states ($V_{ds} = 1$ V) are realized through gradually increasing the light power in the optical write process. b) Continuous and orderly data writing and erasing by varying the laser power and allowing random intermediate states to transition. c) ON/OFF ratio as a function of the erasing voltage (left) and reading voltage (right). d) Circuit diagram for the logic-AND calculation based on the PMS. The circuit is formed by connecting two MoS₂-PZT PMSs in series and using an external 1 G Ω resistor as a load. $P_{in,A}$ and $P_{in,B}$ represent two independent optical inputs, and V_{out} represents the electrical output. e) Truth table of the basic logic-AND calculation. f) Output voltage (V_{out}) at four different combinations of input states: (0, 0), (1, 0), (0, 1), and (1, 1).

barriers at the drain and source terminals also contribute to the separation of the photogenerated electron–hole pairs and reduce their recombination. As a result, more holes are trapped in the MoS₂/PZT interface and induce the strong downward polarization in the PZT to deplete the electrons in the MoS₂ (OFF-state). The reading voltage also has notable influence on the OFF- and ON-state readout currents, as shown in Figure S8 (Supporting Information). It is obvious that a higher reading voltage results in a higher readout current both before and after the optical writing. However, a relatively more substantial OFF-state current change causes the ON/OFF ratio to decrease as

the reading voltage increases (Figure 4c, right). Although a high voltage causes a high current due to Ohm's law, the polarization reversal of the PZT layer at a high bias leads to the change in the resistance of the MoS₂ channel, which is the dominant reason. Except for photonic storage, the PMS can serve as a building block in an integrated logic circuit for photon-triggered logic gates. As shown in Figure 4d, we connect two MoS₂-PZT PMSs in series and use an external 1 G Ω resistor as a load. Two independent focused lasers are used as optical inputs ($P_{in,A}$ and $P_{in,B}$). Before the logic calculation, we conduct an optical erasure process with both PMSs to ensure that they

are in HRSs. Next, we measure the output voltage (V_{out}) of the load at four different combinations of input states: (0, 0), (1, 0), (0, 1), and (1, 1). As shown in Figure 4e,f, this integrated circuit realizes the available photon-triggered logic-AND operation and permanently memorizes the results after their computing. Other binary logic operations can also achieve optical control by designing different integrated circuits based on PMSs.

6. Conclusion

We have demonstrated a photon-memristive system with memristive characteristics that are stimulated by optical inputs. The PMS indicates the relevance between the memristance and number of photon number, that is, continuously tunable resistance depending on the history of photons. Our approach uses a 2D photoelectric semiconductor (MoS_2) that is integrated with a thin ferroelectric (PZT) layer. The memristive characteristics are realized through the mechanism in which the photon-excited charges in the MoS_2 are accumulated near the interface by interfacial engineering creating a vertical field that affects the polarization in the PZT, which modulates the channel resistance in turn. The PMS shows the ability to accomplish multibit photonic storage by the varying laser power, light pulse time, and/or erase/read voltage. A fast optical set/reset, huge resistance-changeable space, and random memorized state switching are beneficial to future high-capacity data storage and in-memory computing. The relevant principle also can be applied to other high-surface area 2D layered materials with good photoresponsivity, such as MoSe_2 , WS_2 , etc., and ferroelectric ultrathin film with low coercive field, such as BiFeO_3 , BaTiO_3 , etc., when they make an available and reasonable match. Our results introduce optical inputs to the memristive system and set the stage for further exciting new developments in photonic information technology.

7. Experimental Section

Growth of Thin PZT film by PLD: Thin $\text{Pb}(\text{Zr}_{0.52}\text{Ti}_{0.48})\text{O}_3$ (PZT) films were grown on the (001)-oriented SrTiO_3 (STO) single-crystal substrates via pulsed-laser deposition with a KrF excimer laser ($\lambda = 248$ nm). The thin PZT films were grown at a temperature of 650 °C in dynamic oxygen pressure of 100 mTorr with a laser energy density of 1 J cm^{-2} and a laser repetition rate of 1 Hz from a ceramic target of composition $\text{Pb}_{1.1}(\text{Zr}_{0.52}\text{Ti}_{0.48})\text{O}_3$. The growth rate was ≈ 0.1 Å s^{-1} , and the thickness of the PZT films was fixed at 10 nm. After the depositions, the films were cooled to 400 °C at a rate of 5 °C min^{-1} and annealed at 760 Torr oxygen for 1 h and then naturally cooled to room temperature.

Growth and Transfer of the MoS_2 Sheet: Monolayer MoS_2 sheets were grown on silicon substrates with 300 nm of SiO_2 using the CVD technique. A quartz boat containing 8 mg of MoO_3 powder ($\geq 99.5\%$, Sigma-Aldrich), which served as a precursor, was positioned in the center of a furnace and the Si/ SiO_2 wafer was placed face down in the boat above the precursor. 300 mg of sulfur ($\geq 99.9\%$, Aladdin) was located outside of the furnace and warmed up by using heating tape. The furnace temperature was increased up to 750 °C at a rate of 15 °C min^{-1} . When the furnace temperature reached 650 °C, the heating tape started working. The highest temperature of 750 °C was held constant for 30 min, and then it was allowed to naturally cool down. The growth occurred under atmospheric pressure with a 10 sccm argon flow.

During the transfer process, first, a thin layer of PMMA (495 K, A11, MicroChem) was spin coated on the SiO_2/Si substrate with monolayer MoS_2 sheets, and then baked for 3 min at 150 °C. Next, the sample coated by PMMA was floated on a 30% hydrofluoric acid solution to etch the SiO_2 layer. Finally, the detached film was cleaned in deionized water several times and transferred to the target substrate (PZT/STO).

PFM Measurements: The polarization observations of the PZT film in different stages were conducted by using single-frequency PFM. PFM imaging was performed by applying an AC bias on the tip, and the amplitude and frequency were controlled as 1 V_{pp} and 300 kHz, respectively. Silicon AFM probes with Pt/Ir conductive coatings were used to detect the bias-induced piezoelectric surface deformation in the contact mode.

Supporting Information

Supporting Information is available from the Wiley Online Library or from the author.

Acknowledgements

K.Z. and D.H.M. contributed equally to this work. This work was supported by NSFC 51872031, National Key R&D Project from Minister of Science and Technology, China (No. 2016YFA0202703).

Conflict of Interest

The authors declare no conflict of interest.

Keywords

logic calculations, MoS_2 -PZT, photonic storage, photon-memristive systems, theoretical derivations

Received: April 2, 2020

Revised: May 5, 2020

Published online:

- [1] M. Li, W. H. P. Pernice, C. Xiong, T. Baehr-Jones, M. Hochberg, H. X. Tang, *Nature* **2008**, 456, 480.
- [2] W. Chen, K. M. Beck, R. Bucker, M. Gullans, M. D. Lukin, H. Tanji-Suzuki, V. Vuletic, *Science* **2013**, 341, 768.
- [3] L. Chua, *IEEE Trans. Circuit Theory* **1971**, 18, 507.
- [4] D. B. Strukov, G. S. Snider, D. R. Stewart, R. S. Williams, *Nature* **2008**, 453, 80.
- [5] A. A. Bessonov, M. N. Kirikova, D. I. Petukhov, M. Allen, T. Ryhänen, M. J. A. Bailey, *Nat. Mater.* **2015**, 14, 199.
- [6] F. Alibart, S. Pleutin, O. Bichler, C. Gamrat, T. Serrano-Gotarredona, B. Linares-Barranco, D. Vuillaume, *Adv. Funct. Mater.* **2012**, 22, 609.
- [7] A. Chanthbouala, V. Garcia, R. O. Cherifi, K. Bouzouhouane, S. Fusil, X. Moya, S. Xavier, H. Yamada, C. Deranlot, N. D. Mathur, M. Bibes, A. Barthélémy, J. Grollier, *Nat. Mater.* **2012**, 11, 860.
- [8] Z. Wen, Di Wu, A. Li, *Appl. Phys. Lett.* **2014**, 105, 052910.
- [9] Yu. V. Pershin, M. Di Ventra, *Phys. Rev. B* **2008**, 78, 113309.
- [10] R. Ge, X. Wu, M. Kim, J. Shi, S. Sonde, Li Tao, Y. Zhang, J. C. Lee, D. Akinwande, *Nano Lett.* **2018**, 18, 434.
- [11] M. Kim, R. Ge, X. Wu, X. Lan, J. Tice, J. C. Lee, D. Akinwande, *Nat. Commun.* **2018**, 9, 2524.

- [12] J. Wang, *Science* **2003**, 299, 1719.
- [13] T. Choi, S. Lee, Y. J. Choi, V. Kiryukhin, S.-W. Cheong, *Science* **2009**, 324, 63.
- [14] N. A. Pertsev, V. G. Kukhar, H. Kohlstedt, R. Waser, *Phys. Rev. B* **2003**, 67, 054107.
- [15] B. E. Park, H. Ishiwara, M. Okuyama, S. Sakai, S. M. Yoon, *Ferroelectric-Gate Field Effect Transistor Memories*, Springer, Netherlands **2016**.
- [16] V. Garcia, M. Bibes, *Nature* **2012**, 483, 279.
- [17] J. Junquera, P. Ghosez, *Nature* **2003**, 422, 506.
- [18] K. S. Novoselov, A. Mishchenko, A. Carvalho, A. H. Castro Neto, *Science* **2016**, 353, aac9439.
- [19] Q. H. Wang, K. Kalantar-Zadeh, A. Kis, J. N. Coleman, M. S. Strano, *Nat. Nanotechnol.* **2012**, 7, 699.
- [20] F. Xia, H. Wang, Di Xiao, M. Dubey, A. Ramasubramaniam, *Nat. Photonics* **2014**, 8, 899.
- [21] W. Jin, P.-C. Yeh, N. Zaki, D. Zhang, J. T. Sadowski, A. Al-Mahboob, A. M. van der Zande, D. A. Chenet, J. I. Dadap, I. P. Herman, P. Sutter, J. Hone, R. M. Osgood, *Phys. Rev. Lett.* **2013**, 111, 106801.
- [22] Y. Zhao, K. Xu, F. Pan, C. Zhou, F. Zhou, Y. Chai, *Adv. Funct. Mater.* **2017**, 27, 1603484.
- [23] O. Lopez-Sanchez, D. Lembke, M. Kayci, A. Radenovic, A. Kis, *Nat. Nanotechnol.* **2013**, 8, 497.
- [24] F. Zhou, J. Chen, X. Tao, X. Wang, Y. Chai, *Research* **2019**, 2019, 9490413.
- [25] K. Zhang, M. Peng, W. Wu, J. Guo, G. Gao, Y. Liu, J. Kou, R. Wen, Y. Lei, A. Yu, Y. Zhang, J. Zhai, Z. L. Wang, *Mater. Horiz.* **2017**, 4, 274.
- [26] C. Ko, Y. Lee, Y. Chen, J. Suh, D. Fu, A. Suslu, S. Lee, J. D. Clarkson, H. S. Choe, S. Tongay, R. Ramesh, J. Wu, *Adv. Mater.* **2016**, 28, 2923.
- [27] H. Li, Q. Zhang, C. C. R. Yap, B. K. Tay, T. H. T. Edwin, A. Olivier, D. Baillargeat, *Adv. Funct. Mater.* **2012**, 22, 1385.
- [28] D. Cao, C. Wang, F. Zheng, W. Dong, L. Fang, M. Shen, *Nano Lett.* **2012**, 12, 2803.
- [29] M.-M. Yang, M. Alexe, *Adv. Mater.* **2018**, 30, 1704908.
- [30] G. De Luca, N. Strkalj, S. Manz, C. Bouillet, M. Fiebig, M. Trassin, *Nat. Commun.* **2017**, 8, 1419.
- [31] K. Zhang, J. Zhai, Z. L. Wang, *2D Mater.* **2018**, 5, 035038.
- [32] S. Bertolazzi, D. Krasnozhan, A. Kis, *ACS Nano* **2013**, 7, 3246.
- [33] K. Zhang, M. Peng, A. Yu, Y. Fan, J. Zhai, Z. L. Wang, *Mater. Horiz.* **2019**, 6, 826.
- [34] Y. C. Wu, C.-H. Liu, S.-Y. Chen, F.-Y. Shih, P.-H. Ho, C.-W. Chen, C.-T. Liang, W.-H. Wang, *Sci. Rep.* **2015**, 5, 11472.
- [35] M. M. Furchi, D. K. Polyushkin, A. Pospischil, T. Mueller, *Nano Lett.* **2014**, 14, 6165.